

# Thresholds in FAPT: Euclid vs Minkowski

Alexander P. Bakulev<sup>a\*</sup>

<sup>a</sup> *Bogoliubov Lab. Theor. Phys., JINR  
Jolio-Curie 6, 141980 Dubna, Russia*

## Abstract

We give a short introduction to the Analytic Perturbation Theory (APT) [1, 2, 3, 4, 5] in QCD, describe its problems and suggest as a tool for their resolution the Fractional APT (FAPT) [6, 7, 8, 9]. We also describe shortly how to treat heavy-quark thresholds in FAPT. As an applications of this technique we discuss (i) the pion form factor calculation in the Euclidean FAPT and (ii) the Higgs boson decay  $H^0 \rightarrow b\bar{b}$  in Minkowskian FAPT. We conclude with comparison of both approaches, Euclidean and Minkowskian FAPT.

## 1 Analytic Perturbation Theory in QCD

In the standard QCD Perturbation Theory (PT) we know that the Renormalization Group (RG) equation  $da_s[L]/dL = -a_s^2 - \dots$  for the effective coupling  $\alpha_s(Q^2) = a[L]/\beta_f$  with  $L = \ln(Q^2/\Lambda^2)$ ,  $\beta_f = b_0(N_f)/(4\pi) = (11 - 2N_f/3)/(4\pi)$ <sup>1</sup>. Then the one-loop solution generates Landau pole singularity,  $a_{(1)}[L] = 1/L$  with subscript  $(l)$  meaning  $l$ -loop order.

In the Analytic Perturbation Theory (APT) we have different effective couplings in Minkowskian (Radyushkin [10] and Krasnikov&Pivovarov [11]) and Euclidean (Shirkov&Solovtsov [3]) regions. In the Euclidean domain,  $-q^2 = Q^2$ ,  $L = \ln Q^2/\Lambda^2$ , APT generates one set of images for the effective coupling and its  $n$ -th powers,  $\{\mathcal{A}_n[L]\}_{n \in \mathbb{N}}$ , whereas in the Minkowskian domain,  $q^2 = s$ ,  $L_s = \ln s/\Lambda^2$ , it generates another set,  $\{\mathfrak{A}_n[L_s]\}_{n \in \mathbb{N}}$ . APT is based on the RG and causality that guarantees standard perturbative UV asymptotics and spectral properties. Power series  $\sum_m d_m a_{(1)}^m[L]$  transforms into non-power series  $\sum_m d_m \mathcal{A}_m[L]$  in APT.

By the analytization in APT for an observable  $f(Q^2)$  we mean the “Källen–Lehman” representation

$$[f(Q^2)]_{\text{an}} = \int_0^\infty \frac{\rho_f(\sigma)}{\sigma + Q^2 - i\epsilon} d\sigma \quad (1)$$

with the spectral density defined through the perturbative result,  $\rho_f(\sigma) = (1/\pi) \mathbf{Im}[f^{\text{pert}}(-\sigma)]$ . This results in different analytic images in Euclidean and Minkowski regions

$$\mathcal{A}_n[L] \equiv \mathbf{A}_E [a^n[L]] = \int_0^\infty \frac{\rho_n(\sigma)}{\sigma + Q^2} d\sigma, \quad (2a)$$

$$\mathfrak{A}_n[L_s] \equiv \mathbf{A}_M [a^n[L]] = \int_s^\infty \frac{\rho_n(\sigma)}{\sigma} d\sigma. \quad (2b)$$

Then in the one-loop approximation spectral density is  $\rho_1^{(1)}(\sigma) = 1/[\ln^2(\sigma/\Lambda^2) + \pi^2]$  and analytic couplings are

$$\mathcal{A}_1^{(1)}[L] = \frac{1}{L} - \frac{1}{e^L - 1}, \quad \mathfrak{A}_1^{(1)}[L_s] = \frac{1}{\pi} \arccos \frac{L_s}{\sqrt{\pi^2 + L_s^2}}, \quad (3)$$

\*e-mail:bakulev@theor.jinr.ru

<sup>1</sup>We use notations  $f(Q^2)$  and  $f[L]$  in order to specify what arguments we mean — squared momentum  $Q^2$  or its logarithm  $L = \ln(Q^2/\Lambda^2)$ , that is  $f[L] = f(\Lambda^2 \cdot e^L)$  and  $\Lambda^2$  is usually referred to  $N_f = 3$  region.

whereas spectral density for the analytic images of the higher powers ( $n \geq 2, n \in \mathbb{N}$ ) is  $\rho_n^{(1)}(s) = (1/(n-1)!) (-d/dL_s)^{n-1} \rho_1^{(1)}(s)$  and analytic images of the higher powers are:

$$\begin{pmatrix} \mathcal{A}_n^{(1)}[L] \\ \mathfrak{A}_n^{(1)}[L_s] \end{pmatrix} = \frac{1}{(n-1)!} \left( -\frac{d}{dL} \right)^{n-1} \begin{pmatrix} \mathcal{A}_1[L] \\ \mathfrak{A}_1^{(1)}[L_s] \end{pmatrix}. \quad (4)$$

## 2 Fractional APT

In the standard QCD PT we have also:

- the factorization procedure in QCD that gives rise to the appearance of logarithmic factors of the type:  $a^\nu[L] L$ ;<sup>2</sup>
- the RG evolution that generates evolution factors of the type:  $B(Q^2) = [Z(Q^2)/Z(\mu^2)] B(\mu^2)$ , which reduce in the one-loop approximation to  $Z(Q^2) \sim a^\nu[L]$  with  $\nu = \gamma_0/(2b_0)$  being a fractional number.

That means that in order to analytize perturbative QCD expressions we need to construct analytic images of new functions:  $a^\nu, a^\nu L^m, \dots$ . The result of this procedure is just the Fractional APT (FAPT). Formally speaking, in order to construct FAPT we need to use formulas (2) with substituting spectral densities with integer indices  $n$ , namely  $\rho_n(\sigma)$ , by corresponding spectral densities  $\rho_\nu(\sigma)$  with fractional indices  $\nu$ . But in the one-loop approximation FAPT can more effectively be constructed using recursive relations (4), see for details in [6, 8]. The explicit expressions for couplings in Euclidean,  $\mathcal{A}_\nu^{(1)}[L]$ , and Minkowskian,  $\mathfrak{A}_\nu^{(1)}[L]$ , domains are

$$\mathcal{A}_\nu^{(1)}[L] = \frac{1}{L^\nu} - \frac{F(e^{-L}, 1-\nu)}{\Gamma(\nu)}; \quad \mathfrak{A}_\nu^{(1)}[L] = \frac{\sin \left[ (\nu-1) \arccos \left( L/\sqrt{\pi^2 + L^2} \right) \right]}{\pi(\nu-1)(\pi^2 + L^2)^{(\nu-1)/2}}. \quad (5)$$

Here  $F(z, \nu)$  is reduced Lerch transcendental function, which is an analytic function in  $\nu$ . Interesting to note that  $\mathcal{A}_\nu^{(1)}[L]$  appears to be an entire function in  $\nu$ , whereas  $\mathfrak{A}_\nu^{(1)}[L]$  is de-

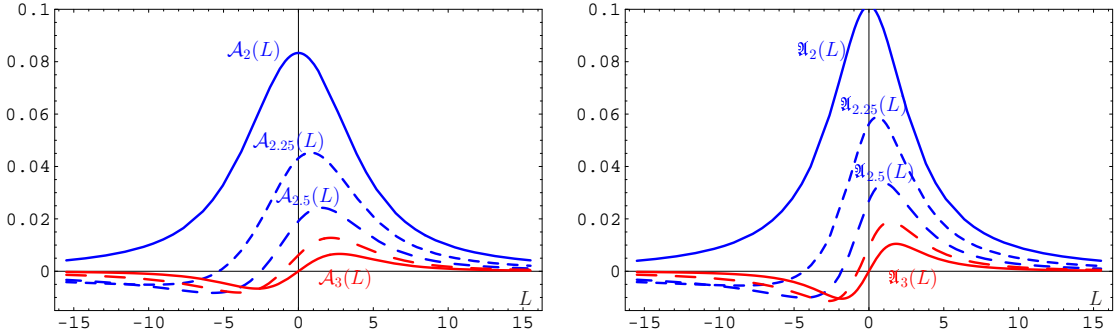


Figure 1: Graphics of  $\mathcal{A}_\nu^{(1)}[L]$  (left panel) and  $\mathfrak{A}_\nu^{(1)}[L]$  (right panel) for fractional  $\nu \in [2, 3]$ .

terminated completely in terms of elementary functions. These couplings have the following properties:

$$\mathcal{A}_0^{(1)}[L] = \mathfrak{A}_0^{(1)}[L] = 1; \quad (6a)$$

$$\mathcal{A}_{-m}^{(1)}[L] = L^m \text{ for } m \in \mathbb{N}; \quad \mathfrak{A}_{-1}^{(1)}[L] = L, \quad \mathfrak{A}_{-2}^{(1)}[L] = L^2 - \frac{\pi^2}{3}, \quad \mathfrak{A}_{-3}^{(1)}[L] = L^3 - \pi^2 L, \dots; \quad (6b)$$

$$\begin{pmatrix} \mathcal{A}_m^{(1)}[L] \\ \mathfrak{A}_m^{(1)}[L] \end{pmatrix} = (-1)^m \begin{pmatrix} \mathcal{A}_m^{(1)}[-L] \\ \mathfrak{A}_m^{(1)}[-L] \end{pmatrix} \text{ for } m \geq 2, m \in \mathbb{N}; \quad (6c)$$

<sup>2</sup>First indication that a special “analytization” procedure is needed to handle these logarithmic terms appeared in [12], where it has been suggested that one should demand the analyticity of the partonic amplitude as a *whole*.

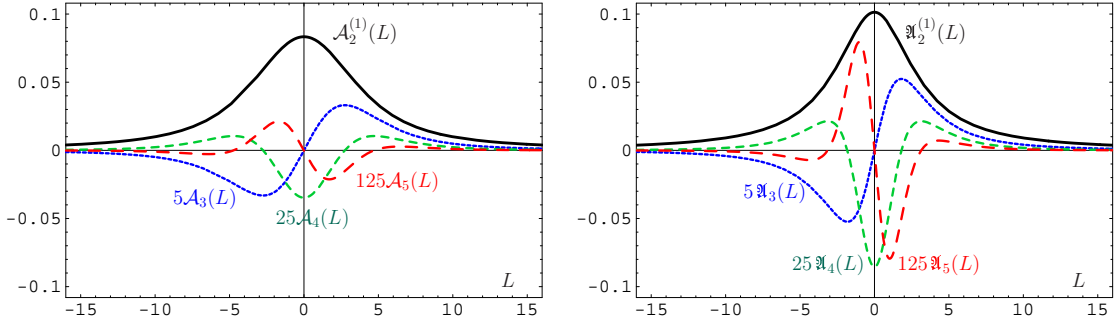


Figure 2: Graphics of  $\mathcal{A}_\nu[L]$  (left panel) and  $\mathfrak{A}_\nu[L]$  (right panel) for integer  $\nu = 2, 3, 4, 5$ . In order to show all curves on the same panel we scale different curves by factors  $5^{\nu-2}$ .

$$\mathcal{A}_m^{(1)}[\pm\infty] = \mathfrak{A}_m^{(1)}[\pm\infty] = 0 \text{ for } m \geq 2, m \in \mathbb{N}; \quad (6d)$$

$$\mathcal{D}^k \begin{pmatrix} \mathcal{A}_\nu^{(l)} \\ \mathfrak{A}_\nu^{(l)} \end{pmatrix} = \frac{d^k}{d\nu^k} \begin{pmatrix} \mathcal{A}_\nu^{(l)} \\ \mathfrak{A}_\nu^{(l)} \end{pmatrix} = \begin{pmatrix} \mathbf{A}_E \\ \mathbf{A}_M \end{pmatrix} \left[ a_{(l)}^\nu \ln^k(a_{(l)}) \right] = \begin{pmatrix} \mathbf{A}_E \\ \mathbf{A}_M \end{pmatrix} \left[ \frac{d^k}{d\nu^k} a_{(l)}^\nu \right]. \quad (6e)$$

We display graphics of  $\mathcal{A}_\nu^{(1)}[L]$  and  $\mathfrak{A}_\nu^{(1)}[L]$  in Fig. 1: one can see here a kind of distorting mirror on both panels. Next, in Fig. 2 we show graphics for  $\nu = 2, 3, 4, 5$ . Here we can trace the partial values

$$\mathcal{A}_2^{(1)}[0] = \frac{1}{12}, \quad \mathcal{A}_4^{(1)}[0] = \frac{-1}{720}, \quad \mathcal{A}_3^{(1)}[0] = \mathcal{A}_5^{(1)}[0] = 0; \quad (7a)$$

$$\mathfrak{A}_2^{(1)}[0] = \frac{1}{\pi^2}, \quad \mathfrak{A}_4^{(1)}[0] = -\frac{1}{3\pi^4}, \quad \mathfrak{A}_3^{(1)}[0] = \mathfrak{A}_5^{(1)}[0] = 0. \quad (7b)$$

Graphics for  $\mathcal{A}_\nu[L]$  as functions of  $\nu$  at fixed values of  $L$  can be found in our last papers [6]. We compare the basic ingredients of FAPT in Table 1 with their counterparts in conventional PT and APT.

Theory	PT	APT	FAPT(E)	FAPT
Space	$\{a^\nu\}_{\nu \in \mathbb{R}}$	$\{\mathcal{A}_m\}_{m \in \mathbb{N}}$	$\{\mathcal{A}_\nu\}_{\nu \in \mathbb{R}}$	$\{\mathfrak{A}_\nu\}_{\nu \in \mathbb{R}}$
Series expansion	$\sum_m f_m a^m[L]$	$\sum_m f_m \mathcal{A}_m[L]$	$\sum_m f_m \mathcal{A}_m[L]$	$\sum_m f_m \mathfrak{A}_m[L]$
Inverse powers	$(a[L])^{-m}$	—	$\mathcal{A}_{-m}[L] = L^m$	$\mathfrak{A}_{-m}[L] = L^m + O(\pi^2)$
Index derivative	$a^\nu \ln^k a$	—	$\mathcal{D}^k \mathcal{A}_\nu$	$\mathcal{D}^k \mathfrak{A}_\nu$
Logarithms	$a^\nu L^k$	—	$\mathcal{A}_{\nu-k}$	$\mathfrak{A}_{\nu-k}$

Table 1: Comparison of PT, APT, and FAPT in Euclidean (FAPT(E),  $L = \ln(Q^2/\Lambda^2)$ ), and Minkowski (FAPT(M),  $L = \ln(s/\Lambda^2)$ ) domains in the one-loop approximation. In the row, named ‘Inverse powers’, we put  $\mathfrak{A}_{-m}[L] = L^m + O(\pi^2)$  that encodes just Eq. (6b).

### 3 Developments of FAPT

#### 3.1 Two-loop coupling

In this section we want to show how good is FAPT in approximating the two-loop analytic coupling expressions by expanding them in non-power series in terms of one-loop analytic couplings.

To this end, we remind the two-loop equation for the normalized coupling  $a_{(2)} = b_0 \alpha / (4\pi)$ :

$$\frac{da_{(2)}[L]}{dL} = -a_{(2)}^2[L] [1 + c_1 a_{(2)}[L]] \quad \text{with } c_1 \equiv \frac{b_1}{b_0^2}. \quad (8)$$

The exact solution  $a_{(2)}[L]$  of this equation satisfies the following functional equation:

$$\frac{1}{a_{(2)}[L]} + c_1 \ln \left[ \frac{a_{(2)}[L]}{1 + c_1 a_{(2)}[L]} \right] = L. \quad (9)$$

Its exact solution is known [13] to be

$$a_{(2)}[L] = -\frac{1}{c_1} \frac{1}{1 + W_{-1}(z_W[L])}, \quad (10)$$

where  $z_W[L] = (1/c_1) \exp(-1 + i\pi - L/c_1)$  and  $W_k$ ,  $k = 0, \pm 1, \dots$ , denote different branches of the Lambert function  $W(z)$ , defined through functional equation  $z = W(z) e^{W(z)}$ . Review of its properties can be found in [14, 13, 15].

To construct FAPT for the two-loop quantities one should use formulas (2) with substituting the spectral densities  $\rho_n(\sigma)$  by the corresponding two-loop spectral densities  $\rho_\nu^{(2)}(\sigma)$ , defined by

$$\rho_\nu^{(2)}(\sigma) = \frac{1}{\pi} \text{Im} \left[ a_{(2)}^\nu[L - i\pi] \right]. \quad (11)$$

Then analytic images in Euclidean,  $\mathcal{A}_\nu^{(2)}[L]$ , and Minkowskian,  $\mathfrak{A}_\nu^{(2)}[L]$ , domains are defined through

$$\mathcal{A}_\nu^{(2)}[L] = \int_0^\infty \frac{\rho_\nu^{(2)}(\sigma)}{\sigma + Q^2} d\sigma, \quad \mathfrak{A}_\nu^{(2)}[L_s] = \int_s^\infty \frac{\rho_\nu^{(2)}(\sigma)}{\sigma} d\sigma. \quad (12)$$

We can also expand  $a_{(2)}[L]$  in terms of  $a_{(1)}[L] = 1/L$  with inclusion of terms  $O(a_{(1)}^3)$ :

$$a_{(2)}[L] = a_{(1)}[L] + c_1 a_{(1)}^2[L] \ln a_{(1)}[L] + c_1^2 a_{(1)}^3[L] (\ln^2 a_{(1)}[L] + \ln a_{(1)}[L] - 1) + \dots \quad (13)$$

and then produce analytic version of this expansion

$$\mathcal{A}_1^{(2); \text{FAPT}}[L] = \mathcal{A}_1^{(1)} + c_1 \mathcal{D} \mathcal{A}_{\nu=2}^{(1)} + c_1^2 (\mathcal{D}^2 + \mathcal{D} - 1) \mathcal{A}_{\nu=3}^{(1)} + \dots \quad (14)$$

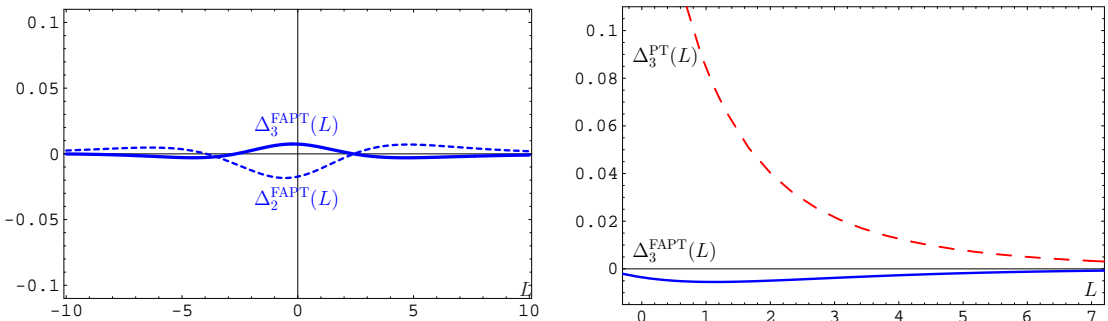


Figure 3: Left panel: Comparison of relative errors  $\Delta_2^{\text{FAPT}}[L]$  (dotted line) and  $\Delta_3^{\text{FAPT}}[L]$  (solid line) in FAPT. Right panel: Comparison of relative errors  $\Delta_3^{\text{PT}}[L]$  (dashed line) in standard PT and  $\Delta_3^{\text{FAPT}}[L]$  (solid line) in FAPT.

In Fig. 3 we demonstrate nice convergence of this expansion using relative errors of the 2- and 3-term approximations:

$$\Delta_2^{\text{FAPT}}[L] = 1 - \frac{\mathcal{A}_1^{(1)}[L] + c_1 \mathcal{D} \mathcal{A}_{\nu=2}^{(1)}[L]}{\mathcal{A}_1^{(2)}[L]}, \quad (15)$$

$$\Delta_3^{\text{FAPT}}[L] = \Delta_2^{\text{FAPT}}[L] - \frac{c_1^2 (\mathcal{D}^2 + \mathcal{D} - 1) \mathcal{A}_{\nu=3}^{(1)}[L]}{\mathcal{A}_1^{(2)}[L]}, \quad (16)$$

$$\Delta_3^{\text{PT}}[L] = 1 - \frac{a_{(1)}[L] + c_1 a_{(1)}^2[L] \ln a_{(1)}[L] + c_1^2 a_{(1)}^3[L] (\ln^2 a_{(1)}[L] + \ln a_{(1)}[L] - 1)}{a_{(2)}[L]}. \quad (17)$$

We see that relative accuracy of the 3-term approximation in FAPT (see the left panel of Fig. 3) is better than 2% for  $L \geq -2$ . In the same time, the right panel of Fig. 3 demonstrates that relative accuracy of the same 3-term approximation in standard PT even at  $L \approx 1$  is much higher — about 10%, whereas in FAPT it is smaller than 1%!

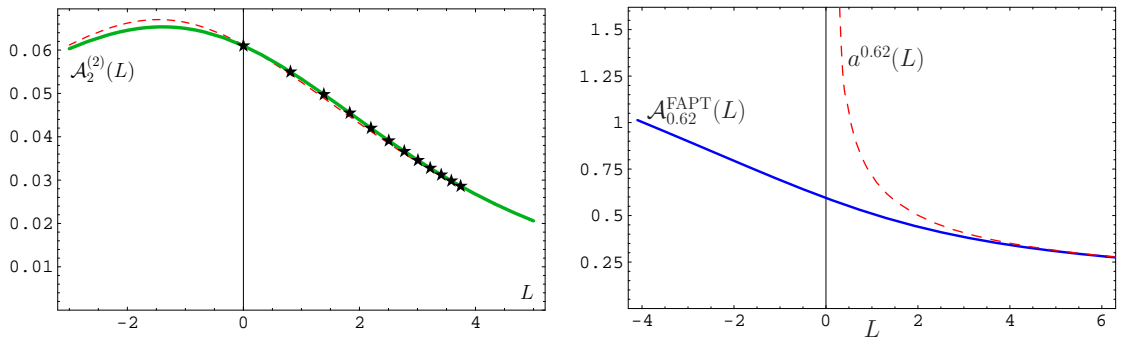


Figure 4: Left panel: The solid line corresponds to  $\mathcal{A}_2^{(2)}[L]$ , computed analytically via Eq. (18); dashed line represents the result of a numerical integration, while stars correspond to the available numerical results of Magradze in [15]. Right panel: The solid line represents  $\mathcal{A}_{0.62}^{(2);FAPT}[L]$ , computed analytically via Eq. (18), while the dashed line stands for  $a_{(2)}^{0.62}[L]$ .

We obtain the corresponding expansion for the two-loop coupling with index  $\nu$ :

$$\mathcal{A}_\nu^{(2);FAPT}[L] = \mathcal{A}_\nu^{(1)}[L] + c_1 \nu \mathcal{D} \mathcal{A}_{\nu+1}^{(1)}[L] + c_1^2 \nu \left[ \frac{\nu+1}{2} \mathcal{D}^2 + \mathcal{D} - 1 \right] \mathcal{A}_{\nu+2}^{(1)}[L] + \dots \quad (18)$$

and display comparison of different results for  $\mathcal{A}_2^{(2);FAPT}[L]$  on the left panel of Fig. 4. On the right panel of this figure we show comparison of FAPT and standard QCD PT with respect to the fractional index (power) of the coupling, fixed at the value  $\nu = 0.62$ , corresponding to the evolution exponent of the second moment of the pion distribution amplitude.

In the Minkowskian region convergence of the FAPT expansion for the two-loop coupling

$$\mathfrak{A}_2^{(2);FAPT}[L] = \mathfrak{A}_2^{(1)}[L] + 2 c_1 \mathcal{D} \mathfrak{A}_{\nu=3}^{(1)}[L] + c_1^2 [3 \mathcal{D}^2 + 2 \mathcal{D} - 2] \mathfrak{A}_{\nu=4}^{(1)}[L] + \dots \quad (19)$$

is also very good, but in the vicinity of the point  $L = 0$  (Landau pole in the standard PT) it is not so fast, so that we need to take into account  $O(c_1^5)$ -terms in order to reach 5% level of accuracy, for more details look in [6].

Now we turn to the corresponding expansion for the two-loop coupling with logarithm:

$$\mathcal{L}_{\nu,1}^{(2)}[L] = \mathbf{A}_E [(a_{(2)})^\nu L] = \mathcal{A}_{\nu-1}^{(2)} + c_1 \mathcal{D} \mathcal{A}_\nu^{(2)} - c_1^2 \mathcal{A}_{\nu+1}^{(2)} + \frac{c_1^3}{2} \mathcal{A}_{\nu+2}^{(2)} - \frac{c_1^4}{3} \mathcal{A}_{\nu+3}^{(2)} + O(c_1^5). \quad (20)$$

The exact spectral density can be easily found,

$$\rho_{\mathcal{L}_{\nu,1}}^{(2)}[L] = \frac{R_{(1)}[L]}{R_{(2)}^\nu[L]} \sin [\nu \varphi_{(2)}[L] - \varphi_{(1)}[L]] \quad (21)$$

with  $R_{(1,2)}[L]$  and  $\varphi_{(1,2)}[L]$  being inverse modula and phases of the corresponding one- and two-loop densities. In Fig. 5 we show the relative deviations

$$\Delta_{3,4}(\mathcal{L}_{1.31,1}) = \frac{\mathcal{L}_{1.31,1}^{(1)} + O(c_1) + O(c_1^2) + O(c_1^3) + O(c_1^4)}{\mathcal{L}_{1.31,1}^{(2)}} - 1. \quad (22)$$

Once again, we see that relative accuracy of the  $O(c_1^4)$  approximation in FAPT is better than

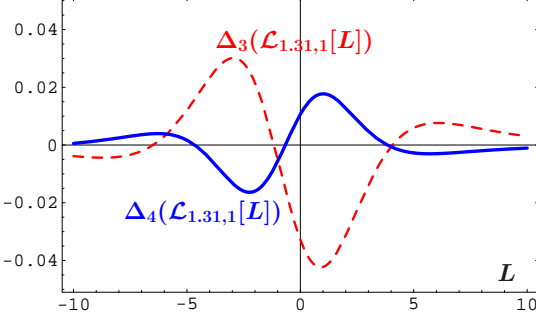


Figure 5: The solid line corresponds to  $\mathcal{A}_2^{(2)}[L]$ , computed analytically via Eq. (18); dashed line represents the result of a numerical integration.

2% for all  $L$  with the largest deviations in the vicinity of the point  $L = 0$ . In the Minkowski region convergence of the FAPT expansion for the corresponding quantity  $\mathcal{L}_{\nu,1}^{(2)}[L]$  is also very good, but not so fast as in the Euclidean case, so that we need to take into account  $O(c_1^5)$ -term in order to reach the same level of accuracy, for more details see in [9].

### 3.2 Heavy-quark thresholds

Construction of FAPT with fixed number of quark flavors,  $N_f$ , is a two-step procedure: we start with the perturbative result  $[a(Q^2)]^\nu$ , generate the spectral density  $\rho_\nu(\sigma) = (1/\pi)\text{Im}[a^\nu(-\sigma)]$ , and then obtain analytic couplings  $\mathcal{A}_\nu[L]$  and  $\mathfrak{A}_\nu[L]$  via Eqs. (6). Here  $N_f$  is fixed and  $N_f$ -dependent coefficient  $b_0(N_f)$  is factorized out. We can proceed in the same manner for  $N_f$ -dependent quantities:  $[\alpha_s(Q^2; N_f)]^\nu \Rightarrow \bar{\rho}_\nu(\sigma; N_f) = \bar{\rho}_\nu[L_\sigma; N_f] \equiv \rho_\nu(\sigma)/\beta_f^\nu \Rightarrow \bar{\mathcal{A}}_\nu[L; N_f]$  and  $\bar{\mathfrak{A}}_\nu[L; N_f]$  — here  $N_f$  is fixed, but not factorized out.

Global version of FAPT, which takes into account heavy-quark thresholds, is constructed along the same lines but starting from global perturbative coupling  $[\alpha_s^{\text{glob}}(Q^2)]^\nu$ , being a continuous function of  $Q^2$  due to choosing different values of QCD scales  $\Lambda_f$ , corresponding to different values of  $N_f$ . We illustrate here the case of only one heavy-quark threshold at  $s = m_4^2$ , corresponding to the transition  $N_f = 3 \rightarrow N_f = 4$ . Then we obtain the discontinuous spectral density

$$\rho_n^{\text{glob}}(\sigma) = \rho_n^{\text{glob}}[L_\sigma] = \theta(L_\sigma < L_4) \bar{\rho}_n[L_\sigma; 3] + \theta(L_4 \leq L_\sigma) \bar{\rho}_n[L_\sigma + \lambda_4; 4], \quad (23)$$

with  $L_\sigma \equiv \ln(\sigma/\Lambda_3^2)$ ,  $L_f \equiv \ln(m_f^2/\Lambda_3^2)$  and  $\lambda_f \equiv \ln(\Lambda_3^2/\Lambda_f^2)$  for  $f = 4$ , which is expressed in terms of fixed-flavor spectral densities with 3 and 4 flavors,  $\bar{\rho}_n[L; 3]$  and  $\bar{\rho}_n[L + \lambda_4; 4]$ . However it generates the continuous Minkowskian coupling

$$\begin{aligned} \mathfrak{A}_\nu^{\text{glob}}[L_s] &= \theta(L_s < L_4) \left( \bar{\mathfrak{A}}_\nu[L_s; 3] - \bar{\mathfrak{A}}_\nu[L_4; 3] + \bar{\mathfrak{A}}_\nu[L_4 + \lambda_4; 4] \right) \\ &+ \theta(L_4 \leq L_s) \bar{\mathfrak{A}}_\nu[L_s + \lambda_4; 4]. \end{aligned} \quad (24)$$

and the analytic Euclidean coupling (for more detail see in [9])

$$\mathcal{A}_\nu^{\text{glob}}[L] = \bar{\mathcal{A}}_\nu[L + \lambda_4; 4] + \int_{-\infty}^{L_4} \frac{\bar{\rho}_\nu[L_\sigma; 3] - \bar{\rho}_\nu[L_\sigma + \lambda_4; 4]}{1 + e^{L - L_\sigma}} dL_\sigma. \quad (25)$$

We analyze now how important is the deviation of the global FAPT from fixed  $N_f$  FAPT. In the Euclidean domain we may write

$$\mathcal{A}_\nu^{\text{glob}}[L] = \bar{\mathcal{A}}_\nu[L + \lambda_4; 4] + \Delta\bar{\mathcal{A}}_\nu[L] \quad (26)$$

with

$$\Delta\bar{\mathcal{A}}_\nu[L] \equiv \int_{-\infty}^{L_4} \frac{\bar{\rho}_\nu[L_\sigma; 3] - \bar{\rho}_\nu[L_\sigma + \lambda_4; 4]}{1 + e^{L - L_\sigma}} dL_\sigma, \quad (27)$$

whereas in the Minkowski domain —

$$\mathfrak{A}_\nu^{\text{glob}}[L] = \bar{\mathfrak{A}}_\nu[L + \lambda_4; 4] + \Delta\bar{\mathfrak{A}}_\nu[L] \quad (28)$$

with

$$\Delta\bar{\mathfrak{A}}_\nu[L] \equiv \theta(L < L_4) \left[ \bar{\mathfrak{A}}_\nu[L; 3] - \bar{\mathfrak{A}}_\nu[L_4; 3] + \bar{\mathfrak{A}}_\nu[L_4 + \lambda_4; 4] - \bar{\mathfrak{A}}_\nu[L + \lambda_4; 4] \right] \quad (29)$$

In Fig. 6 we show the relative values of deviations in Euclidean and Minkowski domains. We

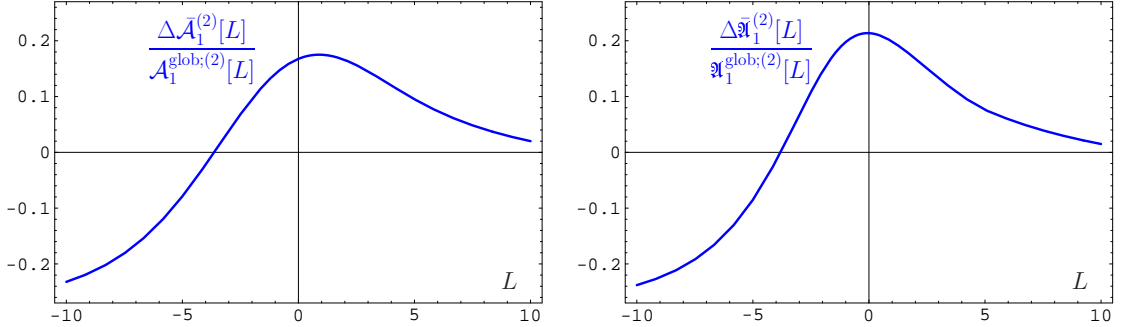


Figure 6: Relative deviations of global coupling with respect to fixed- $N_f$  coupling in APT. Solid lines correspond to the ratios  $\Delta\bar{\mathcal{A}}_1[L]/\mathcal{A}_1^{\text{glob};(2)}[L]$  (left panel) and  $\Delta\bar{\mathfrak{A}}_1[L]/\mathfrak{A}_1^{\text{glob}}[L]$  (right panel).

see that in both domains deviations vary from  $-20\%$  at large values of  $-L \approx 10$ , in the vicinity of  $L \approx -5$  they go through the zero, then grow up to the value  $+20\%$  which is reached at  $L \approx 0$ , and then tends to 0 at  $L \rightarrow \infty$ .

## 4 Electromagnetic pion form factor at NLO

The scaled hard-scattering amplitude truncated at the next-to-leading order (NLO) and evaluated at renormalization scale  $\mu_R^2 = \lambda_R Q^2$  reads [16, 17, 18, 19]

$$T_{\text{H}}^{\text{NLO}}(x, y; \mu_F^2, Q^2) = \frac{\alpha_s(\lambda_R Q^2)}{Q^2} t_{\text{H}}^{(0)}(x, y) + \frac{\alpha_s^2(\lambda_R Q^2)}{4\pi Q^2} t_{\text{H}}^{(1)}(x, y; \mu_F^2/Q^2) \quad (30)$$

with shorthand notation ( $\bar{x} \equiv 1 - x$ )

$$t_{\text{H}}^{(1)}(x, y; \mu_F^2/Q^2) = C_F t_{\text{H}}^{(0)}(x, y) 2 \left( 3 + \ln(\bar{x}\bar{y}) \right) \ln \frac{Q^2}{\mu_F^2} + b_0 t_{\text{H}}^{(1,\beta)}(x, y; \lambda_R) + t_{\text{H}}^{(\text{FG})}(x, y). \quad (31)$$

The leading twist-2 pion distribution amplitude (DA) [20] at normalization scale  $\mu_F^2$  is given by [21]

$$\varphi_\pi(x, \mu_F^2) = 6x(1-x) \left[ 1 + a_2(\mu_F^2) C_2^{3/2}(2x-1) + a_4(\mu_F^2) C_4^{3/2}(2x-1) + \dots \right]. \quad (32)$$

All nonperturbative information is encapsulated in Gegenbauer coefficients  $a_n(\mu_F^2)$ .

To obtain factorized part of pion form factor (FF) one needs to convolute the pion DA with the hard-scattering amplitude:

$$F_\pi^{\text{Fact}}(Q^2) = \varphi_\pi(x; \mu_F^2) \otimes \underset{x}{T_H^{\text{NLO}}} (x, y; \mu_F^2, Q^2) \otimes \varphi_\pi(y; \mu_F^2). \quad (33)$$

In order to obtain the analytic expression for the pion FF at NLO in [22] the so-called “Naive Analytization” has been suggested. It uses analytic image only for coupling itself,  $\mathcal{A}_1^{(2)}$ , but not for its powers. In contrast and in full accord with the APT ideology the receipt of “Maximal Analytization” has been proposed recently in [23]. The corresponding expressions for the analytized hard amplitudes read as follows:

$$[Q^2 T_H(x, y, Q^2)]_{\text{Nai-An}} = \mathcal{A}_1^{(2)}(\lambda_R Q^2) t_H^{(0)}(x, y) + \frac{(\mathcal{A}_1^{(2)}(\lambda_R Q^2))^2}{4\pi} t_H^{(1)}\left(x, y; \lambda_R, \frac{\mu_F^2}{Q^2}\right) \quad (34)$$

$$[Q^2 T_H(x, y, Q^2)]_{\text{Max-An}} = \mathcal{A}_1^{(2)}(\lambda_R Q^2) t_H^{(0)}(x, y) + \frac{\mathcal{A}_2^{(2)}(\lambda_R Q^2)}{4\pi} t_H^{(1)}\left(x, y; \lambda_R, \frac{\mu_F^2}{Q^2}\right). \quad (35)$$

In Fig. 7 we show the predictions for the factorized pion FF in the standard pQCD and

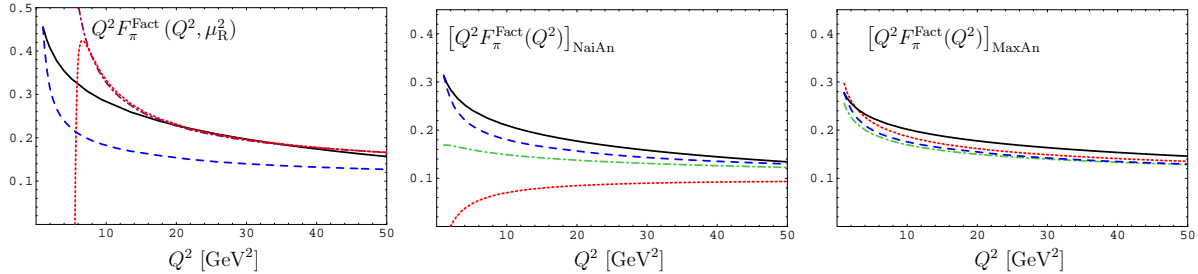


Figure 7: Left panel: Factorized pion FF in the standard  $\overline{\text{MS}}$  scheme. The solid line corresponds to the scale setting  $\mu_R^2 = 1 \text{ GeV}^2$ , dashed line — to  $\mu_R^2 = Q^2$ , dotted lines — to the principle of minimal sensitivity, whereas dash-dotted lines — to the principle of fastest apparent convergency. Central panel: Factorized pion FF in the “Naive Analytization”. Right panel: Factorized pion FF in the “Maximal Analytization”. On both panels solid lines correspond to the scale setting  $\mu_R^2 = 1 \text{ GeV}^2$ , dashed lines — to  $\mu_R^2 = Q^2$ , dotted lines — to the BLM [24] prescription, whereas dash-dotted lines — to the  $\alpha_V$ -scheme.

in “Naive” and in the “Maximal Analytization” approaches. We see that in the “Maximal Analytization” approach the obtained results are practically insensitive to the renormalization scheme and scale-setting choice (already at the NLO level).

We show also the graphics for the whole pion FF, obtained in APT with the “Maximally Analytic” procedure using the Ward identity to match the non-factorized and factorized parts of the pion FF, see the right panel of Fig. 7. The green strip in this figure contains both nonperturbative uncertainties from nonlocal QCD sum rules [25, 26, 27] and renormalization scheme and scale ambiguities at the level of the NLO accuracy.

It is interesting to note here that the FAPT approach, used in [7] for analytization of the  $\ln(Q^2/\mu_F^2)$ -terms in the hard amplitude (30), diminishes also the dependence on the factorization scale setting in the interval  $\mu_F^2 = 1 - 50 \text{ GeV}^2$ .

This conclusion starts to be even more pronounced in the complete FAPT analysis of the factorized pion FF. Indeed, if we put  $\mu_F^2 = Q^2$  then we obtain in the pion FF convolutions with  $\varphi_\pi(x, Q^2)$  which contains ERBL evolution factors  $a_{2n}(\mu_0^2) [\alpha_s(Q^2)/\alpha_s(\mu_0^2)]^{\nu_{2n}}$  with  $\nu_{2n}(N_f) = \gamma_0(2n)/(2b_0(N_f))$ . Numerically  $\nu_2 = 0.62 - 0.72$  and  $\nu_4 = 0.90 - 1.06$ . In  $T_H^{\text{NLO}}(x, y, Q^2)$  we have three types of contributions:  $\alpha_s(Q^2)$ ,  $\alpha_s^2(Q^2)$ , and  $b_0(N_f)\alpha_s^2(Q^2)$ . The scheme of “analytization” of  $N_f$ -dependent quantity is the same as in the case of the global approach, see in Fig. 8. Indeed,

we start with  $b_0(N_f)\alpha_s^\nu(Q^2)$ , obtain corresponding spectral density  $\rho_{\nu;b_0}^{\text{glob}}(\sigma)$ , being in case of the single heavy-quark threshold of the type

$$\rho_{\nu;b_0}^{\text{glob}}(\sigma) = \rho_{\nu;b_0}^{\text{glob}}[L_\sigma] = \theta(L_\sigma < L_4) b_0(3) \bar{\rho}_n[L_\sigma; 3] + \theta(L_4 \leq L_\sigma) b_0(4) \bar{\rho}_n[L_\sigma + \lambda_4; 4], \quad (36)$$

and then construct corresponding analytic image  $\mathcal{A}_{\nu;b_0}^{\text{glob}}[L]$ , using integral representations (2).

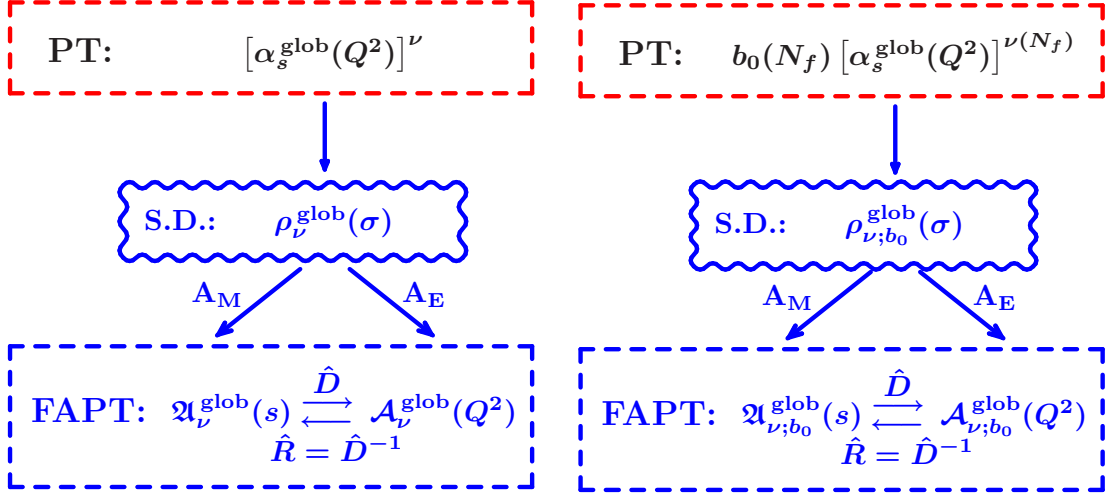


Figure 8: Schemes of ‘analytization’ of  $N_f$ -dependent quantities. On the left panel the starting object to analytize is  $[\alpha_s^{\text{glob}}(Q^2)]^\nu$ , whereas on the right panel —  $b_0(N_f)[\alpha_s^{\text{glob}}(Q^2)]^\nu$ .

In Fig. 9 we show the predictions for the factorized pion FF in the complete FAPT approach with different settings for  $\mu_F$  (see figure caption for details) and for comparison — in the ‘Maximal Analytization’ scheme with  $\mu_F^2 = Q^2$ . We see that both approaches produce practically the same results.

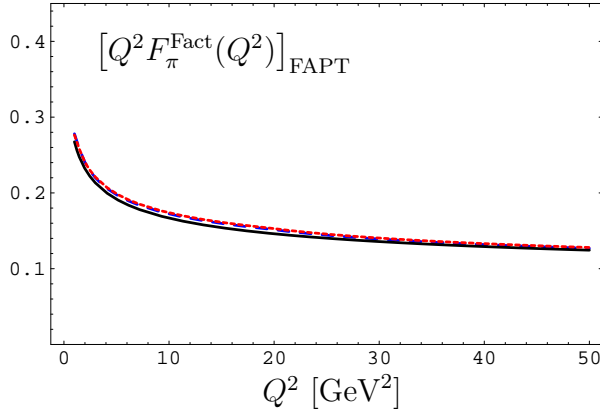


Figure 9: Factorized pion FF in the complete FAPT approach. The solid line corresponds to the factorization scale  $\mu_F^2 = Q^2$ , dashed line — to  $\mu_F^2 = 6 \text{ GeV}^2$ , whereas dotted line — to the ‘Maximal Analytization’ with  $\mu_F^2 = Q^2$ .

We conclude this section with the note that in the Euclidean domain taking thresholds and  $N_f$ -dependence of coefficients into account generates tiny correction! The main advantage of the complete FAPT approach: There are no problems with thresholds. Bonus: Pion FF automatically appears to be analytic function out of the Minkowski cut [9]. Note here that in this case one should use in the Minkowski region not the coupling  $\mathcal{A}_\nu(s)$ , but instead the analytic image of the Euclidean coupling on the lower side of the cut, namely,  $\mathcal{A}_\nu(-s - i0) = \text{Re } \mathcal{A}_\nu(s) + i\pi\rho_\nu(s)$ . In contrast to the real coupling  $\mathcal{A}_\nu(s)$ , this quantity naturally generates an imaginary part of the pion form factor, which is measured in  $e^+e^- \rightarrow \pi^+\pi^-$  reactions.

## 5 Higgs boson decay into $b\bar{b}$ pair in FAPT

In this section we analyze the Higgs boson decay to a  $b\bar{b}$  pair. For the decay width we have

$$\Gamma_{H \rightarrow b\bar{b}}(M_H) = \frac{G_F}{4\sqrt{2}\pi} M_H \tilde{R}_S(M_H^2) \quad \text{with} \quad \tilde{R}_S(M_H^2) \equiv m_b^2(M_H^2) R_S(M_H^2) \quad (37)$$

and  $R_S(s)$  is the  $R$ -ratio for the scalar correlator, see for details in [8, 28]. The running mass  $m(Q^2)$  is described in the three-loop approximation by the renormgroup equation [9]

$$m_{(3)}^2(Q^2) = \hat{m}_{(3)}^2 [\alpha_s(Q^2)]^{\nu_0} [1 - \delta_{21} \alpha_s]^{\nu_{21}} [1 + \delta_{22} \alpha_s]^{\nu_{22}}, \quad (38)$$

with RG-invariant mass  $\hat{m}_{(3)}^2$  (for  $b$ -quark  $\hat{m}_{b;(3)} \approx 8$  GeV) and  $\nu_0 = 1.04$ ,  $\delta_{21} = 0.672$ ,  $\nu_{21} = -0.743$ ,  $\delta_{22} = 0.029$ , and  $\nu_{22} = 8.59$  at  $N_f = 5$ .

In the standard PT direct multi-loop calculations are usually performed in the Euclidean region for the corresponding Adler function  $D_S = 3 [1 + \sum_{n>0} d_n \alpha_s^n(Q^2)]$ , where QCD perturbation theory works. Functions  $D_S$  and  $R_S(s) = 3 [1 + \sum_{n>0} r_n \alpha_s^n(s)]$  can be related to each other via a dispersion relation without any reference to perturbation theory. This generates relations between  $r_n$  and  $d_n$  coefficients, involving the famous  $\pi^2$ -terms due to integral transformation of  $\ln^k(Q^2/\mu^2)$  in  $d_n$ :

$$\mathfrak{A}_{-2}[L] = L^2 - \frac{\pi^2}{3}, \quad \mathfrak{A}_{-3}[L] = L (L^2 - \pi^2), \quad \dots$$

The influence of these  $\pi^2$ -terms can be substantial, as has been shown by Baikov *et al.* [28].

### 5.1 Comparing different approaches to calculate $\Gamma_{H \rightarrow b\bar{b}}(M_H)$

We compare now the results of different approaches to calculate  $\tilde{R}_S(M_H^2)$ .

- Baikov *et al.* (BCK) [28] used standard QCD PT at the  $O(a_s^4)$ -order with  $\Lambda_{N_f=5}^{(4)} = 231$  MeV:

$$\tilde{R}_S^{(l=4)\text{BCK}}(s) = 3m_{(l=4)}^2(s) \left[ 1 + \sum_{n \geq 1}^4 r_n(5) \left( \frac{\alpha_s^{(l=4)}}{\pi} \right)^n \right]. \quad (39)$$

- Broadhurst *et al.* (BKM) [29] in the approach of the so-called “Naive Non-Abelianization” (NNA) used the “contour-improved” optimization of power expansion. Their formulas are very closed to the one-loop FAPT (see more detailed discussion in [8, 30]):

$$\tilde{R}_S^{(l=1)\text{FAPT}}(s) = 3\hat{m}_{(l=1)}^2 \left[ \mathfrak{A}_{\nu_0}^{(1);\text{glob}}(s) + \sum_{n \geq 1}^4 d_n(5) \frac{\mathfrak{A}_{n+\nu_0}^{(1);\text{glob}}(s)}{\pi^n} \right]. \quad (40)$$

We show the prediction obtained in this approach with using  $\Lambda_{N_f=5}^{(1);Z} = 111$  MeV (extracted from condition  $\mathfrak{A}_1^{(1);\text{glob}}(m_Z^2) = 0.120$ ) by the dotted (green) line in Fig. 10. It appears to be lower than the standard PT result (dashed red line) by  $\approx 8\%$ .

- In the FAPT approach with “freezed” at the value  $d_n(5)$  coefficients  $d_n(N_f)$  (as also has been done in the BCK and BKM approaches) we define  $\mathfrak{B}_{n+\nu_0}(s)$  as the analytic images of  $\alpha_s^{n+\nu_0}(Q^2)[1 + \delta_1 \alpha_s(Q^2)]^{\nu_1}$  in the Minkowski region and obtain

$$\tilde{R}_S^{(3)\text{FAPT}(5)}(s) = 3\hat{m}_b^2 \left[ \mathfrak{B}_{\nu_0}^{(3);\text{glob}}(s) + \sum_{n \geq 1}^3 d_n(5) \frac{\mathfrak{B}_{n+\nu_0}^{(3);\text{glob}}(s)}{\pi^n} \right]. \quad (41)$$

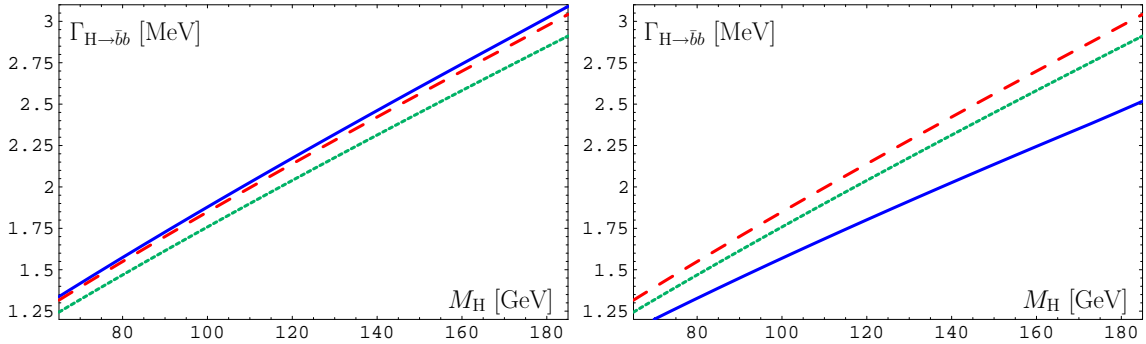


Figure 10: Results of calculations of  $\Gamma_{H \rightarrow \bar{b}b}(M_H^2)$  in different approaches. On both panels dashed (red) lines display the BCK results and dotted (green) lines — the BKM results. Solid line on the left panel corresponds to the results obtained in the FAPT approach with freezed coefficients  $d_n = d_n(N_f = 5)$ , whereas on the right panel — to the results of the complete FAPT approach.

The corresponding predictions for the value  $\Lambda_{N_f=5}^{(3)} = 220$  MeV (being in accord with the last analysis of precision electroweak data by the LEP Collaboration [31] and normalized to  $\mathfrak{A}_1^{(3); \text{glob}}(m_Z^2) = 0.118$ ) are represented in the left panel of Fig. 10 by the solid (blue) line. We see that it is very close to the BCK curve (difference is of the order of 1.5%, and as compared with three-loop BCK result — even of the order of 1%).

- In the complete FAPT approach with the complete analytization of  $N_f$ -dependencies we obtain

$$\tilde{R}_S^{(3)\text{FAPT}}(s) = 3\hat{m}_b^2 \left[ \mathfrak{B}_{\nu_0}^{(3); \text{glob}}(s) + \sum_{n \geq 1}^l \frac{\mathfrak{B}_{n+\nu_0; d_n}^{(3); \text{glob}}(s)}{\pi^n} \right], \quad (42)$$

where the analytic images  $\mathfrak{B}_{n+\nu_0; d_n}(s)$  absorb all  $N_f$ -dependence of  $d_n$  coefficients. Here  $\Lambda_{N_f=5}^{(3)} = 227$  MeV in order to match  $R(m_Z^2)$  value by the LEP Collaboration [31] in the complete FAPT approach: for this reason  $\mathfrak{A}_1^{(3); \text{glob}}(m_Z^2) = 0.119$  and differs slightly from the “freezed” FAPT value  $\mathfrak{A}_1^{(3); \text{glob}}(m_Z^2) = 0.118$ . The results of this approach are shown in the right panel of Fig. 10 by the solid (blue) line and appear to be smaller than the “freezed” results. This difference varies from 14% (at  $M_H = 50$  GeV) to 18% (at  $M_H = 150$  GeV).

We can conclude from this comparison that the standard pQCD power series and the FAPT non-power series expansions appears to be quite close to each other in the region  $L \gg 1$  in the scenario with “freezed” coefficients  $d_n(N_f)$ , corresponding to the value  $N_f = 5$ . The complete FAPT setup, which bears in mind the whole  $N_f$  dependence of the perturbative results, naturally generates another, in our case smaller, result. This is not a surprise, because such an analytization approach effectively average coefficients  $d_n(N_f)$  in the regions with different  $N_f$  values, resulting in reductions of their values and, hence, of the whole non-power series sum. In order to make this effect more transparent we define effective coefficients, corresponding to the complete FAPT series  $\tilde{R}_S^{(3)\text{FAPT}}[L]$  as follows:

$$d_n^{\text{eff}}[L] = \frac{\mathfrak{B}_{n+\nu_0; d_n}^{(3); \text{glob}}[L]}{\mathfrak{B}_{n+\nu_0}^{(3); \text{glob}}[L]}. \quad (43)$$

In Table 2, we show these effective coefficients: one can immediately realize that they indeed diminished by 16 to 18%. Physically this effect of the complete analytization of  $\tilde{R}_S(s)$  corresponds

Table 2: The effective coefficients  $d_n^{\text{eff}}[L]$ , see (43), at  $L = 11 - 13$ . In two last columns we show the corresponding values of  $\tilde{R}_S^{(3)}[L]$  in cases of the “freezed” and the complete FAPT.

	$n = 0$	$n = 1$	$n = 2$	$n = 3$	$\tilde{R}_S^{(3); \text{FAPT}(5)}[L]$	$\tilde{R}_S^{(3); \text{FAPT}}[L]$
$d_n(N_f = 5)$	1.00	5.67	42.0	353	—	—
$d_n^{\text{eff}}[L = 10]$	0.85	4.93	36.4	296	32.44	27.78
$d_n^{\text{eff}}[L = 11]$	0.83	4.80	34.9	276	29.11	24.41
$d_n^{\text{eff}}[L = 12]$	0.82	4.66	33.2	252	26.38	21.64

to taking into account contributions of loops with  $t$ -quarks even in the region  $\sqrt{s} \leq 175$  GeV, where in the standard pQCD in the  $\overline{\text{MS}}$ -scheme only quarks  $u, d, s, c$ , and  $b$  contribute. We see that this effect is sizable.

## 6 Concluding Remarks

We conclude with the following resume:

- The implementation of the analyticity concept (the dispersion relations) from the level of the coupling and its powers to the level of QCD amplitudes as a whole generates extension of the APT to FAPT.
- The rules how to apply FAPT at the two- and three-loop levels are formulated.
- The convergence of the perturbative expansion is significantly improved when using non-power FAPT expansion;
- We formulate the rules how to account for heavy-quark thresholds in FAPT.
- As an additional advantage we obtain the minimal sensitivity to both the renormalization and factorization scale setting, revealed on the example of the pion electromagnetic form factor. Threshold problem (how to fix the value of  $b_0(N_f)$  in the  $O(\alpha_s^2)$ -term) resolved. The result of the complete FAPT prescription appears to be very close to the result of the Brodsky–Lepage–Mackenzie prescription, see in Figs. 7 and 9.
- In application to decay  $H^0 \rightarrow b\bar{b}$  we revealed that the complete FAPT analytization prescription reduces the results by  $\approx 16\%$  as compared with the “freezed” FAPT ones.

The comparison of FAPT in Euclidean and Minkowski regions, done in Sections 2 and 3, shows us close analogy between the two regions—the effect, named by Shirkov and Solovtsov as effect of “distorting mirror”. But the results of the complete FAPT applications to the analysis of the pion form factor in the Euclidean domain (Section 4) and of the Higgs boson decay width in the Minkowski domain (Section 5) are formally quite different: For the pion form factor case the complete FAPT prescription generates approximately the same result as standard FAPT with “freezed”  $N_f$ -dependent terms [23, 7], see in Fig. 9, whereas for the Higgs boson decay this approach generates reduction of the order of 16%.

In order to explain these difference we analyzed the Adler function  $D_S(Q^2)$  with the same perturbative coefficients  $d_n(N_f)$ . Then we revealed that the magnitude of the corresponding reduction of the complete FAPT results in the Euclidean region in comparison with the “freezed” FAPT ones is of the same order (18%) as in the Minkowski case. This demonstration proves that the magnitude of this reduction is related with the strong dependence of perturbative coefficients  $d_n(N_f)$  on  $N_f$  and not with specific character of analytization procedure in the Minkowski region.

## Acknowledgments:

I would like to thank my colleagues and coauthors Sergey Mikhailov and Nico Stefanis for helpful discussions and support, and Konstantin Chetyrkin, Andrei Kataev, and Alexei Pivovarov for stimulating discussions during the International Seminar “Quarks-2008” (Sergiev Posad, Russia, 23–29 May, 2008). This investigation was supported in part by the Deutsche Forschungsgemeinschaft (Projects DFG 436 RUS 113/881/0), the Heisenberg–Landau Programme, grant 2008, the Russian Foundation for Fundamental Research, grants No. 06-02-16215, 07-02-91557, and 08-01-00686, and the BRFBR–JINR Cooperation Programme, contract No. F06D-002.

## References

- [1] H. F. Jones and I. L. Solovtsov, Phys. Lett. **B349**, 519 (1995).
- [2] H. F. Jones, I. L. Solovtsov, and O. P. Solovtsova, Phys. Lett. **B357**, 441 (1995).
- [3] D. V. Shirkov and I. L. Solovtsov, JINR Rapid Commun. **2[76]**, 5 (1996) [arXiv: hep-ph/9604363]; Phys. Rev. Lett. **79**, 1209 (1997); Theor. Math. Phys. **150**, 132 (2007) [arXiv: hep-ph/0611229].
- [4] K. A. Milton and I. L. Solovtsov, Phys. Rev. **D55**, 5295 (1997).
- [5] I. L. Solovtsov and D. V. Shirkov, Phys. Lett. **B442**, 344 (1998).
- [6] A. P. Bakulev, S. V. Mikhailov, and N. G. Stefanis, Phys. Rev. **D72**, 074014 (2005); Erratum: Phys. Rev. **D72**, 119908(E) (2005).
- [7] A. P. Bakulev, A. I. Karanikas, and N. G. Stefanis, Phys. Rev. **D72**, 074015 (2005).
- [8] A. P. Bakulev, S. V. Mikhailov, and N. G. Stefanis, Phys. Rev. **D75**, 056005 (2007). Erratum: Phys. Rev. **D77**, 079901(E) (2008).
- [9] A. P. Bakulev, arXiv:0805.0829 [hep-ph] (to be published in Phys. Part. Nucl.).
- [10] A. V. Radyushkin, JINR Rapid Commun. **78**, 96 (1996). [JINR Preprint, E2-82-159, 26 Febr. 1982; arXiv: hep-ph/9907228].
- [11] N. V. Krasnikov and A. A. Pivovarov, Phys. Lett. **B116**, 168 (1982).
- [12] A. I. Karanikas and N. G. Stefanis, Phys. Lett. **B504**, 225 (2001). Erratum: Phys. Lett. **B636**, 330 (2006).
- [13] B. A. Magradze, Int. J. Mod. Phys. **A15**, 2715 (2000).
- [14] R. Corless *et al.*, Adv. Comput. Math. **5**, 329 (1996).
- [15] B. A. Magradze, Dubna preprint E2-2000-222, 2000 [arXiv: hep-ph/0010070]; Preprint RMI-2003-55, 2003 [arXiv: hep-ph/0305020].
- [16] R. D. Field, R. Gupta, S. Otto, and L. Chang, Nucl. Phys. **B186**, 429 (1981).
- [17] F. M. Dittes and A. V. Radyushkin, Sov. J. Nucl. Phys. **34**, 293 (1981).
- [18] E. Braaten and S.-M. Tse, Phys. Rev. **D35**, 2255 (1987).
- [19] B. Melić, B. Nižić, and K. Passek, Phys. Rev. **D60**, 074004 (1999).
- [20] A. V. Radyushkin, Dubna preprint P2-10717, 1977 [arXiv: hep-ph/0410276].

- [21] A. V. Efremov and A. V. Radyushkin, Phys. Lett. **B94**, 245 (1980).
- [22] N. G. Stefanis, W. Schroers, and H.-C. Kim, Phys. Lett. **B449**, 299 (1999); Eur. Phys. J. **C18**, 137 (2000).
- [23] A. P. Bakulev, K. Passek-Kumerički, W. Schroers, and N. G. Stefanis, Phys. Rev. **D70**, 033014 (2004). Erratum: Phys. Rev. **D70**, 079906(E) (2004).
- [24] S. J. Brodsky, G. P. Lepage, and P. B. Mackenzie, Phys. Rev. **D28**, 228 (1983).
- [25] A. P. Bakulev, S. V. Mikhailov, and N. G. Stefanis, Phys. Lett. **B508**, 279 (2001). Erratum: Phys. Lett. **B590**, 309 (2004).
- [26] A. P. Bakulev and A. V. Pimikov, Acta Phys. Polon. **B37**, 3627 (2006); PEPAN Lett. **4**, 637 (2007) [arXiv: hep-ph/0608288].
- [27] A. P. Bakulev, in *New Trends in High-Energy Physics, Proceedings of the Conference, Yalta (Crimea), 16–23 Sept., 2006*, edited by P. N. Bogolyubov *et al.* (BITP NASU (Kiev), JINR (Dubna), Kiev, 2006), pp. 203–212 [arXiv: hep-ph/0611139].
- [28] P. A. Baikov, K. G. Chetyrkin, and J. H. Kühn, Phys. Rev. Lett. **96**, 012003 (2006).
- [29] D. J. Broadhurst, A. L. Kataev, and C. J. Maxwell, Nucl. Phys. **B592**, 247 (2001).
- [30] A. L. Kataev and V. T. Kim, in *Proceedings of International Seminar on Contemporary Problems of Elementary Particle Physics, Dedicated to the Memory of I. L. Sovtsov, Dubna, January 17–18, 2008.*, edited by A. P. Bakulev *et al.* (JINR, Dubna, 2008), pp. 167–182 [arXiv:0804.3992 (hep-ph)].
- [31] J. Alcaraz *et al.*, arXiv:0712.0929 (hep-ex).